JTTEE5 13:248-264
DOI: 10.1361/10599630419373
1059-9630/$19.00 © ASM International

Peer Reviewed

Analysis of Particle Dynamics and Heat Transfer in Detonation Thermal Spraying Systems

K. Ramadan and P. Barry Butler

(Submitted 29 January 2003; in revised form 14 May 2003)

A computational study of pulsed detonation thermal spraying is conducted using an axisymmetric two-dimensional transient gaseous detonation model. The variations of the particle velocity and temperature at impact on the target surface with the particle initial loading location are analyzed for different conditions. The geometry of the system and the loading locations of the particulate phase are key parameters in pulsed detonation thermal spraying. Since the process is extremely transient and the gas phase experiences a wide range of transient stages all on a timescale of a millisecond, the particle characteristics are strongly dependent on the instantaneous location in the gas stream. One cycle of detonation thermal spraying occurs on a time scale on the order of a millisecond due to the high gas velocities associated with detonation. Thus, a precise control of the process variable parameters is required to have a successful detonation coating process.

Keywords gas-solid, particle loading, pulsed detonation, shock wave

1. Introduction

Pulsed detonation thermal spraying (PDTS) is a coating process in which powdered materials are deposited on a substrate (i.e., surface to be coated) utilizing the high-energy concentration and extreme gas velocities associated with the detonation phenomena. The powder material is accelerated and heated by the carrier gas prior to deposition on the target surface. Upon impact on the target surface, the powder material undergoes plastic deformation to form platelet-shaped particles that adhere to the surface and form a protective coating layer.

An important feature of this method of spraying is the high particle velocity that can be achieved (~1000 m/s).[1,2] This produces coating structures with low porosity, high hardness, and high wear resistance. Another important feature of the detonation coating process is that it is intermittent in nature. This cyclical application process keeps the sprayed substrates at low temperature, typically around 100 °C.[2,3]

A typical gas detonation coating process consists of the following stages.[1,2] A reactive gas mixture (e.g., oxygen and acetylene) is first fed through a mixing chamber into a tubular barrel closed at one end (Fig. 1a). Simultaneously, a powdered material is injected into the barrel through a powder feeder. Combustion of the gas mixture is triggered by a spark plug near the closed end of the tube (Fig. 1b). This leads to a transition from deflagration where the combustion wave propagates at subsonic speed, to detonation where the combustion wave propagates at supersonic speed in the reactants. The detonation wave is characterized as a high-pressure reactive shock wave that is self-supporting due to the release of chemical energy from the reactive gas mixture. The wave propagates downstream in the tube toward the open end of the tube and thus accelerates the powder particles as it passes. The collision of the high-velocity, high-temperature powder particles with the substrate forms a high-density coating with strong adhesion and low porosity. Following the detonation front is an expansion wave that propagates rearward toward the breech end of the tube (Fig. 1b). Once the shock front exits the barrel, it starts decaying and the gas suddenly expands outside the barrel. Depending on the stand-off distance (SOD) defined as the distance between the barrel exit and the substrate, the shock wave can reach the substrate with a large pressure ratio. Once the shock wave strikes the workpiece, it reflects back into the path of the incoming particles (Fig. 1c) where the reflected shock may interact with the particles, depending on the particle size, particle initial loading location as well as other particle properties. The particles continue their path toward the target surface. The impact of the particles on the target surface causes the particles to adhere to the surface forming a circular-splat of coating. A new gas-powder charge is fed into the barrel and the cycle is repeated again.

While the process of detonation coating has been fairly well characterized through years of laboratory experience, there is still a need to develop analytical tools for understanding the interaction between controllable process variables (e.g., chemical composition of detonable gas, particle thermal properties, injection parameters, and particle size distribution) and characteristics of the resultant thermal coating. Most of the theoretical work on PDTS was performed using the one-dimensional Euler equations with constant gas properties.[1,4] A thorough review of the state of the current knowledge of thermal spraying was recently performed by Fauchais et al.[5] The theoretical studies on PDTS cited therein were all based on the one-dimensional flow assumption, and they concluded that much work is necessary to

K. Ramadan and **P. Barry Butler,** Department of Mechanical and Industrial Engineering, The University of Iowa, Iowa City, IA52242. Contact e-mail: Khalid-Ramadan@uiowa.edu, Patrick-Butler@uiowa.edu.

Nomenclature

C	specific heat of particulate phase, J/kg K
C_p	specific heat at constant pressure, J/kg K
C_v	specific heat at constant volume, J/kg K
C_d	drag coefficient
d	tube diameter, m
d_p	particle diameter, μm
D	detonation wave speed, m/s
e	specific internal energy, J/kg
E	total energy per unit volume, J/m^3
h	specific enthalpy, J/kg
h_{conv}	convective heat transfer coefficient, J/s m^2 K
k	gas thermal conductivity, J/s mK
L	tube length, m
L_f	latent heat of fusion, J/kg
m	mass, kg
MW_i	molecular weight of species i
Nu	Nusselt number
P	Pressure, bar
Pr	Prandtl number
r	tube radius, m
Re_p	particle Reynolds number
R_u	universal gas constant, J/kmol K
R	gas constant (= R_u /MW)
t	time, ms
T	temperature, K
u	velocity component in the axial direction, m/s
v	velocity component in the radial direction, m/s
Y_i	mass fraction of species i
Q	heat of reaction, J/kg
x_i	axial loading location, m
x	axial direction
y_i	radial loading location, m
y	radial direction
$\vec{V}$	velocity vector

Greek Letters

β	reaction progress variable
γ	specific heat ratio
δ	the Dirac Delta function
Γ	ratio of specific enthalpy to internal energy
μ	gas dynamic viscosity, N s/m^2
ω	chemical reaction rate, kg/m^3 s
ρ	density, kg/m^3
ε	liquid fraction
ε_p	particle emissivity
σ*	Stefan-Boltzmann constant (= 5.669 × 10^{-8} J/s m^2 K^4)

Subscripts

conv	convection
g	gas
l	liquid
m	melting point
mix	mixture
P	particle
Prod	products
rad	radiation
react	reactants
s	solid

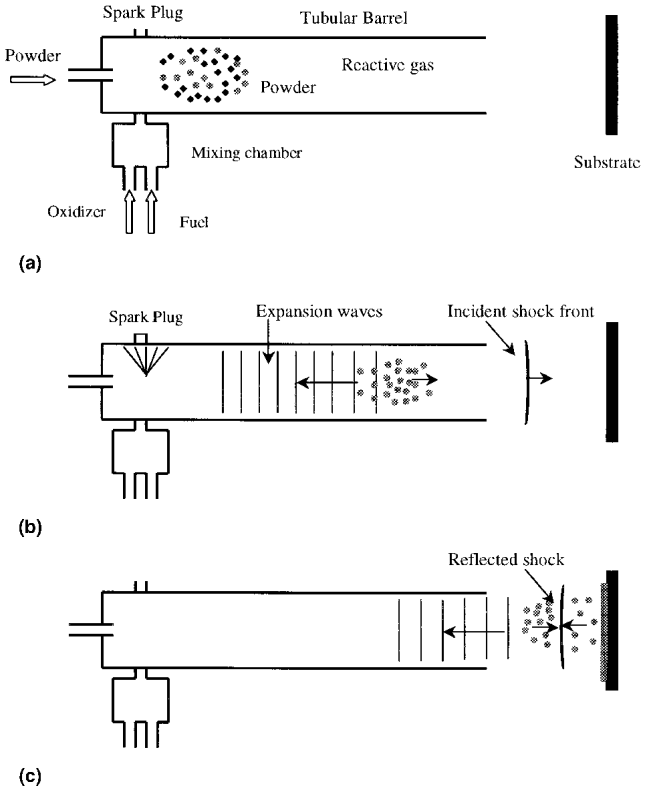

Fig. 1 A typical cycle and sequence of events in detonation thermal spraying (Adapted from Ref. 1 and 2)

better understand the phenomena of the pulsed detonation thermal spraying. However, the analysis of the gas expansion process and interaction with the surroundings, the shock wave decay and shock reflection in PDTS cannot be justified using the one-dimensional flow assumption, where the implementation of the proper boundary conditions at the substrate is not possible with this assumption, and consequently the analysis of the PDTS process using the one-dimensional flow assumption can lead to unrealistic analysis. A realistic multidimensional flow model is thus required to develop a better understanding of pulsed detonation thermal spraying and the phenomena associated with it. The work performed herein addresses this issue through the development of a transient, multicomponent compressible, two-dimensional axisymmetric flow model.

2. Mathematical Model

The process of pulsed detonation thermal spraying is a complex multiphase reactive flow that involves combustion chemistry, shock wave formation and propagation, detonation attenuation, particle transport, shock wave decay, and shock interaction with the substrate. The presence of fast chemical reactions, detonation wave dynamics, and the associated discontinuities in the fluid properties make this problem numerically challenging. The computations of the PDTS process also involve large computational domains with open-ended boundaries and the implementation of numerical boundary conditions.[6] The gas-solid system

in pulsed detonation thermal spraying is normally of dilute character, where the particulate phase exists only to the extent that it does not significantly affect the gas phase characteristics. This is so since if particles exist to a large extent in the detonable gas mixture this may result in severe detonation attenuation or even detonation failure, which consequently leads to failure of the PDTS process or low-quality coatings.

The gas and particulate phase governing equations in this work are represented in a Eulerian and Lagrangian reference frames, respectively. The gas flow is assumed inviscid compressible, where the viscous effects are confined only to the interaction between the gas and the particles. The chemical reaction is assumed to take place in a one-step irreversible process. The particulate phase is assumed to be very sparse that it has no effect on the gas phase. In this case one talks about a one-way coupling between the gas and the particulate phases. The gas-phase governing equations thus reduce to the reactive Euler equations:

$$\frac{\partial \rho}{\partial t} + \frac{\partial (\rho u)}{\partial x} + \frac{\partial (\rho v)}{\partial y} = -\frac{\rho v}{y} \quad \text{(Eq 1)}$$

$$\frac{\partial (\rho u)}{\partial t} + \frac{\partial (\rho u^2 + P)}{\partial x} + \frac{\partial (\rho uv)}{\partial y} = -\frac{\rho uv}{y} \quad \text{(Eq 2)}$$

$$\frac{\partial (\rho v)}{\partial t} + \frac{\partial (\rho uv)}{\partial x} + \frac{\partial (\rho v^2 + P)}{\partial y} = -\frac{\rho v^2}{y} \quad \text{(Eq 3)}$$

$$\frac{\partial E}{\partial t} + \frac{\partial [u(E+P)]}{\partial x} + \frac{\partial [v(E+P)]}{\partial y} = -\frac{v(E+P)}{y} \quad \text{(Eq 4)}$$

$$\frac{\partial (\rho \beta)}{\partial t} + \frac{\partial (\rho u \beta)}{\partial x} + \frac{\partial (\rho v \beta)}{\partial y} = -\frac{\rho v \beta}{y} + \omega_\beta \quad \text{(Eq 5)}$$

In the above equation, x and y are respectively, the axial and radial coordinates in an axisymmetric coordinate system. u, v are the velocity components in x, and y directions, t is the time, ρ is the density, P the pressure, β is a reaction progress variable that takes a value between 0 and 1 such that $\beta = 0$ indicates reactants, $\beta = 1$ products, and $0 < \beta < 1$ indicates the reaction zone. The reaction rate ω_β in Eq 5 is given by

$$\omega_\beta = \frac{|P - P_o|}{P} \frac{\rho}{T_r} (1 - \beta)^{2/3}$$

where P_o is the initial uncompressed gas pressure. The parameter T_r is a constant and represents a typical time associated with the chemical reaction. The total energy E in Eq 4 is given by

$$E = \rho e + \frac{1}{2}\rho(u^2 + v^2) - \rho\beta Q = \frac{P}{\Gamma - 1} + \frac{1}{2}\rho(u^2 + v^2) - \rho\beta Q \quad \text{(Eq 6)}$$

where Q is the energy release due to the chemical reaction, e is the specific internal energy, and Γ is the ratio of specific enthalpy to internal energy given by

$$\Gamma = \Gamma(T) = \frac{h}{e} = \frac{\int_0^T C_p(\xi)d\xi}{\int_0^T C_v(\xi)d\xi} \quad \text{(Eq 7)}$$

In this work the gas is assumed to be thermally perfect and the equation of state is thus:

$$P = \rho R T = \rho[C_p(T) - C_v(T)]T = \rho[\gamma(T) - 1]C_v(T)T \quad \text{(Eq 8)}$$

where C_p, C_v are the gas specific heats at constant pressure and constant temperature, respectively, and $\gamma(T)$ is the specific heat ratio:

$$\gamma(T) = C_p(T)/C_v(T) \quad \text{(Eq 9)}$$

In a one-way coupling where the particulate phase has no effect on the gas phase, it is adequate to study the dynamics of a single particle in the gas stream of the detonation products. The particulate phase governing equations adapted from Ref 7, 8, and 9 are given by

$$\frac{dx_p}{dt} = u_p \quad \text{(Eq 10)}$$

$$\frac{dy_p}{dt} = v_p \quad \text{(Eq 11)}$$

$$\frac{du_p}{dt} = \frac{3}{4}\frac{\partial}{\rho_p d_p} C_d |\vec{V} - \vec{V}_p|(u - u_p) \quad \text{(Eq 12)}$$

$$\frac{dv_p}{dt} = \frac{3}{4}\frac{\rho}{\rho_p d_p} C_d |\vec{V} - \vec{V}_p|(v - v_p) \quad \text{(Eq 13)}$$

$$\frac{dT_p}{dt} = \frac{6}{\rho_p d_p C^*}[h_{conv} + \varepsilon_p \sigma^*(T + T_p)(T^2 + T_p^2)](T - T_p) \quad \text{(Eq 14)}$$

where ε_p and σ^* are, respectively, the particle emissivity, and the Stefan-Boltzmann constant. The latent heat release due to phase change is accounted for in Eq 14 using the effective capacitance method as given by Gross et al.[10]:

$$C^* = C + L_f \delta(T - T_m, \Delta T_m) \quad \text{(Eq 15)}$$

where L_f is the latent heat, T_m is the melting temperature, ΔT_m is a narrow temperature range about T_m over which phase change occurs, and δ is the Dirac Delta function that has a finite value in the range ΔT_m and zero outside. An approximation to the Delta function is given by

$$\delta = \frac{1}{\Delta T_m^2} \max(0, \Delta T_m - |T - T_m|) \quad \text{(Eq 16)}$$

The particle specific heat is given by

$$C = \varepsilon_l C_l + (1 - \varepsilon_l) C_s \quad \text{(Eq 17)}$$

where C_l and C_s are the particle specific heat in the liquid and solid states respectively, ε_l is the fraction of the particle that is melted, which may be derived from the above approximation of the Dirac Delta function and assuming a linear variation of the particle liquid fraction with temperature, where the isothermal

phase change is assumed to take place over a narrow temperature interval about the melting point:

$$\varepsilon_l = \begin{cases} 0, & T_p < T_m - \Delta T_m \\ (T_p - T_m + \Delta T_m)/(2\Delta T_m), & T_m - \Delta T_m \le T_p \le T_m + \Delta T_m \\ 1, & T_p > T_m + \Delta T_m \end{cases} \quad \text{(Eq 18)}$$

C_d in Eq 12 and 13 is the drag coefficient. There are many formulas for the drag coefficient available in literature. Chang et al.[11] reported that employing different drag laws in gas-solid systems results in only small quantitative differences. For micron-sized particles in dusty detonation, the particle slip velocity is normally small (except at the passage of the detonation front), and the following formula for C_d (although derived from incompressible flow relations) is most commonly found in the literature of dusty detonations[9,12] and is thus used in this work:

$$C_d = \begin{cases} 24/Re_p, & Re_p < 1 \\ (24/Re_p)(1 + 0.15\, Re_p^{0.687}), & 1 \le Re_p \le 10^3 \\ 0.44, & Re_p > 10^3 \end{cases} \quad \text{(Eq 19)}$$

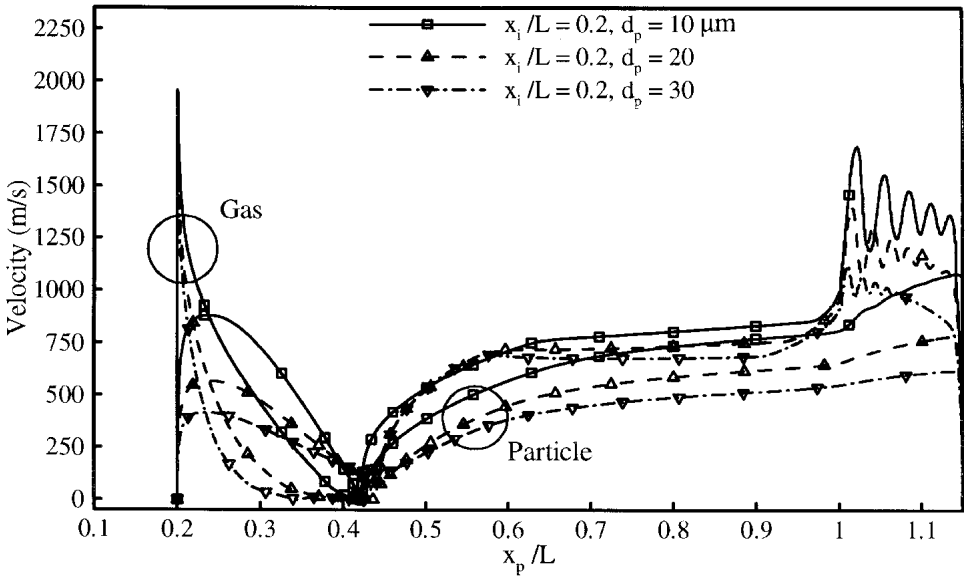

Fig. 2 Particle velocity versus its axial location, and gas velocity at the particle location for axial loading distance $x_i/L = 0.2$ and radial loading distance $y_i/r = 0.05$ (L = 1.0 m, SOD = 6d)

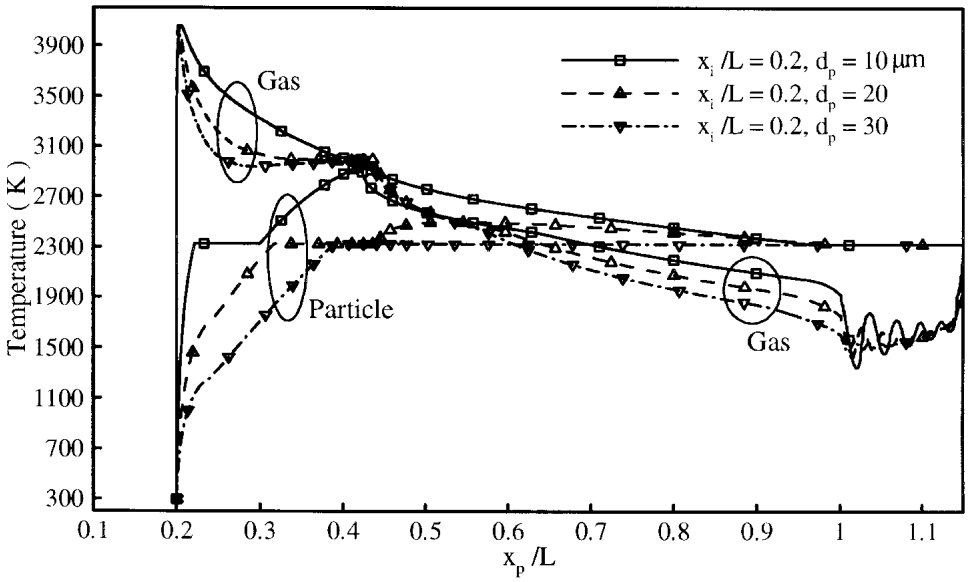

Fig. 3 Particle temperature versus its axial location, and gas temperature at the particle location for axial loading distance $x_i/L = 0.2$ and radial loading distance $y_i/r = 0.05$ (L = 1.0 m, SOD = 6d)

where Re_p is the Reynolds number based on the slip velocity and is defined as

$$Re_p = \frac{\rho|\vec{V} - \vec{V}_p|d_p}{\mu} \quad \text{(Eq 20)}$$

h_{conv} in Eq 14 is the convective heat transfer coefficient given by

$$h_{conv} = \frac{Nuk}{d_p} \quad \text{(Eq 21)}$$

and Nu in the above equation is the Nusselt number given by the following relation:

$$Nu = 2 + 0.6Re_p^{1/2}Pr^{1/3} \quad \text{(Eq 22)}$$

Pr is the Prandtl number:

$$Pr = C_p\mu/k \quad \text{(Eq 23)}$$

where μ and k are the gas viscosity and thermal conductivity.

The gas phase thermal properties are calculated based on the

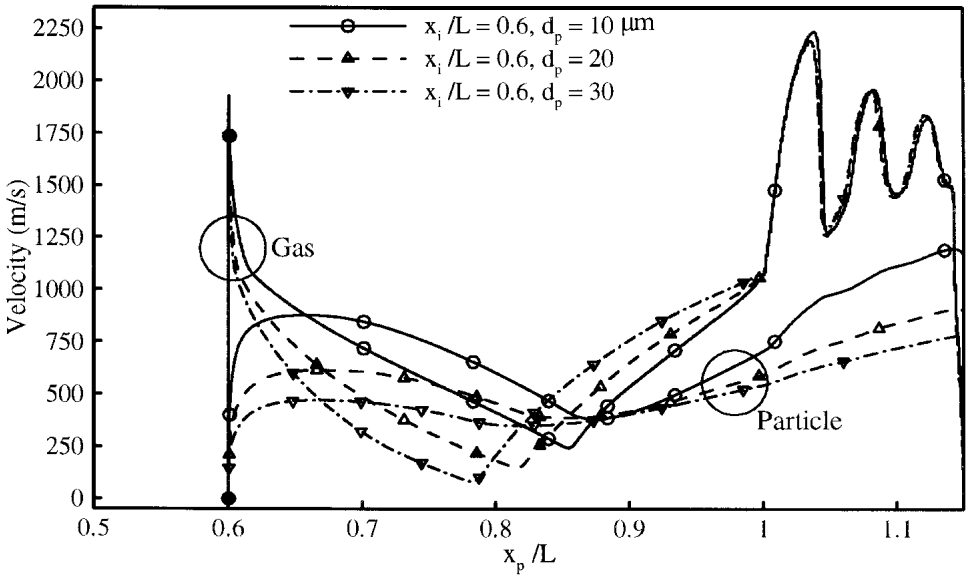

Fig. 4 Particle velocity versus its axial location and gas velocity at the particle location for axial loading distance $x_i/L = 0.6$ and radial loading distance $y_i/r = 0.05$ ($L = 1.0$ m, SOD = $6d$)

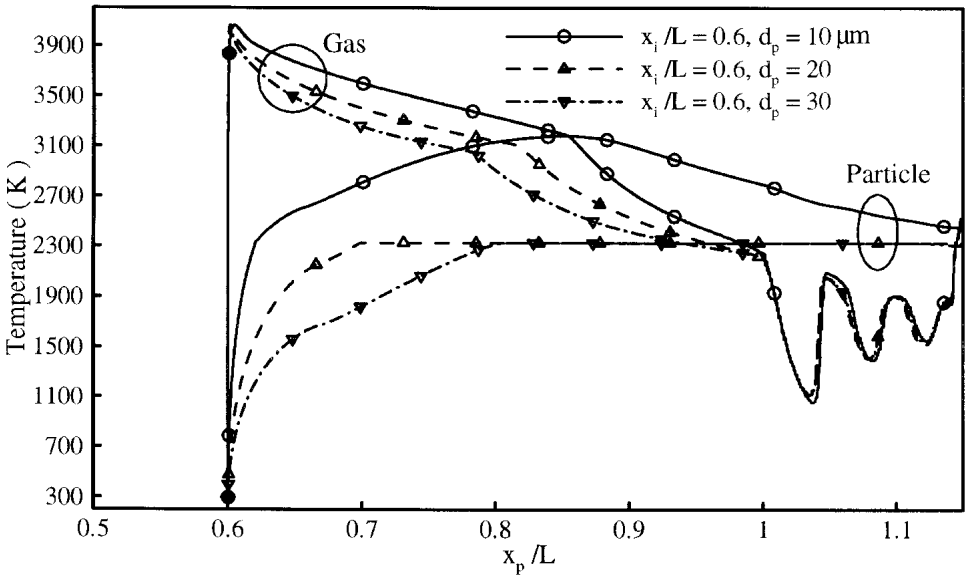

Fig. 5 Particle temperature versus its axial location, and gas temperature at the particle location for axial loading distance $x_i/L = 0.6$ and radial loading distance $y_i/r = 0.05$ ($L = 1.0$ m, SOD = $6d$)

assumption of local chemical equilibrium. The mass fractions of the combustion products are calculated from a chemical equilibrium code[13] that utilizes the Gibbs free energy minimization method. The JANAF tables[14] are then used to curve-fit the specific heats of each constituent of the mixture in a sixth-order polynomial of the form:

$$C_{pi} = a_{oi} + a_{1i}T + a_{2i}T^2 + a_{3i}T^3 + a_4T^4 + a_5T^5 + a_{6i}T^6 \quad \text{(Eq 24)}$$

$$C_{vi} = C_{pi} - R_u/MW_i \quad \text{(Eq 25)}$$

for a temperature range from 298.15 to 4500 K. The mixture specific heats are then calculated using the following formulas:

$$C_p = \sum_i Y_i C_{pi}, \quad C_v = C_p - R_u/MW_{mix}, \quad MW_{mix} = \frac{1}{\sum_i Y_i/MW_i} \quad \text{(Eq 26)}$$

The polynomial constants for the gas mixture are found by substituting Eq 24 into Eq 26:

$$a_j = \sum_i a_{ji} Y/_i, \quad j = 0, 1, 2, \ldots, 6 \quad \text{(Eq 27)}$$

The above relations apply directly to the reactants as well as the products. However, in the reaction zone both the reactants

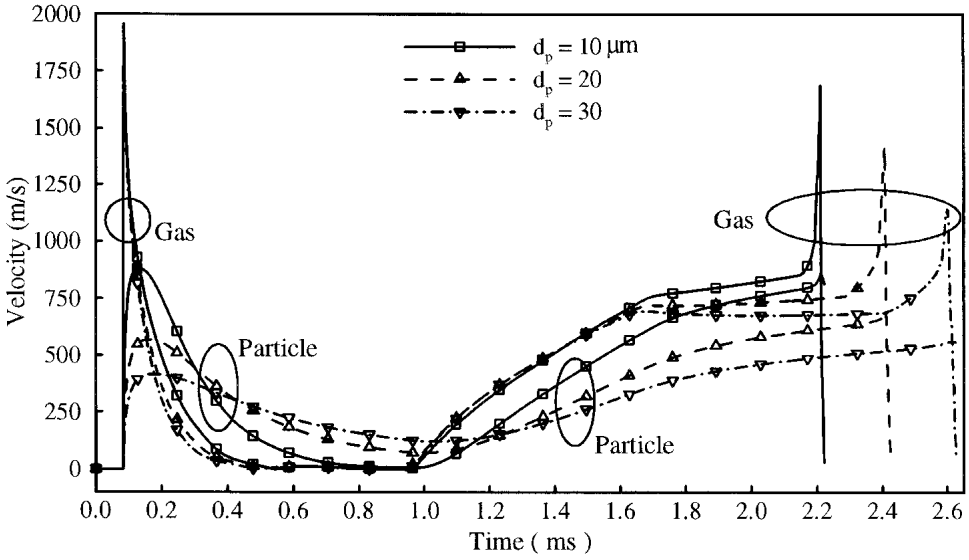

Fig. 6 Particle velocity versus time and gas velocity at the particle location for axial loading distance $x_i/L = 0.2$ and radial loading distance $y_i/r = 0.05$ (L = 1.0 m, SOD = 1d)

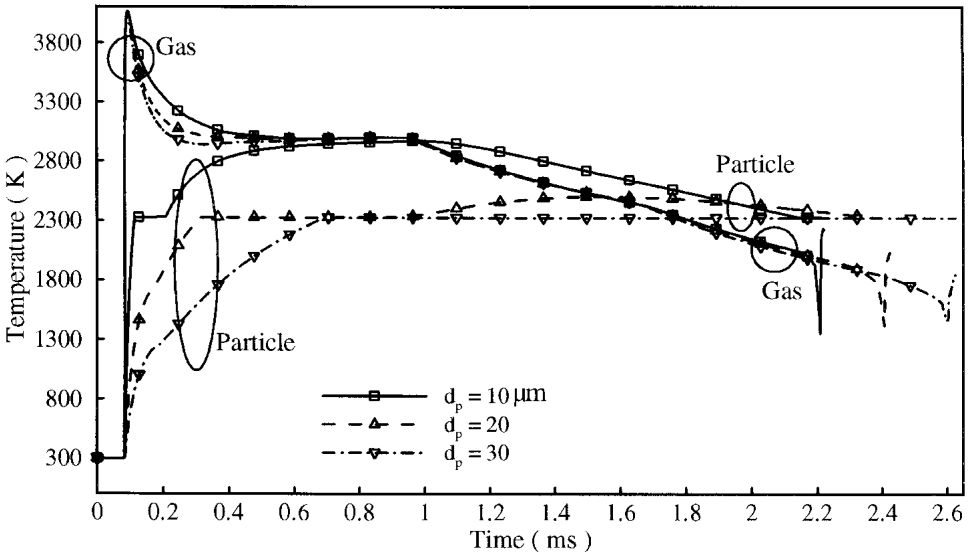

Fig. 7 Particle temperature versus time and gas temperature at the particle location for axial loading distance $x_i/L = 0.2$ and radial loading distance $y_i/r = 0.05$ (L = 1.0 m, SOD = 1d)

and products coexist. In this case, the specific heats are weighted by the mass fractions of the reactants and the products through the reaction progress variable:

$$C_p = \beta C_{p,Prod} + (1-\beta)C_{p,React},\ C_v = \beta C_{v,Prod} + (1-\beta)C_{v,React} \quad \text{(Eq 28)}$$

The viscosity and thermal conductivity of the gas mixture are computed from the corresponding values of the individual species using the Wilke rule.[15,16] The gas phase viscosity and thermal conductivity are then fitted to the following equations:

$$\mu = (b_0 + b_1 T^{b2}) \times 10^{-5}\ \text{N s/m}^2 \quad \text{(Eq 29)}$$

$$k = (c_0 + c_1 T^{c2}) \times 10^{-2}\ \text{J/smK} \quad \text{(Eq 30)}$$

where b_0, b_1, b_2, c_0, c_1, c_2 are constants calculated upon curve-fitting the data. The values of the gas viscosity and thermal conductivity in the reaction zone are weighted by the mass fraction of the reactants and products in the same way as the specific heats (Eq 28).

The particulate phase material used in this work is aluminum oxide (Al_2O_3) with the following properties[6]:

$T_m = 2327$ K, $\rho_p = 3924$ kg/m^3, $C_l = 775$ J/kg K
$C_s = 1887.6$ J/kg K

$L_f = 1.09 \times 10^6$ J/kg, $\varepsilon_p = 0.19$

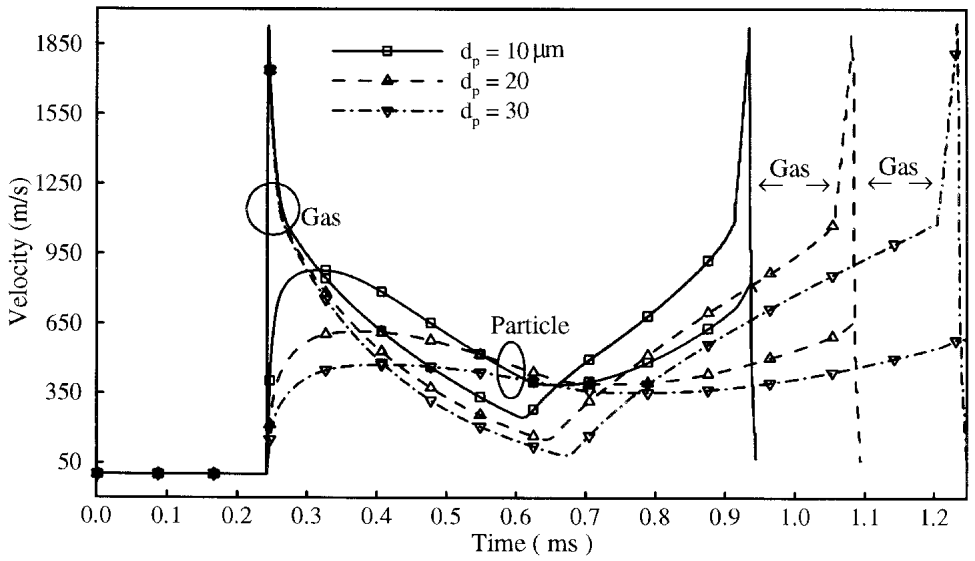

Fig. 8 Particle velocity versus time and gas velocity at the particle location for axial loading distances $x_i/L = 0.6$ and radial loading distance $y_i/r = 0.05$ ($L = 1.0$ m, SOD = 1d)

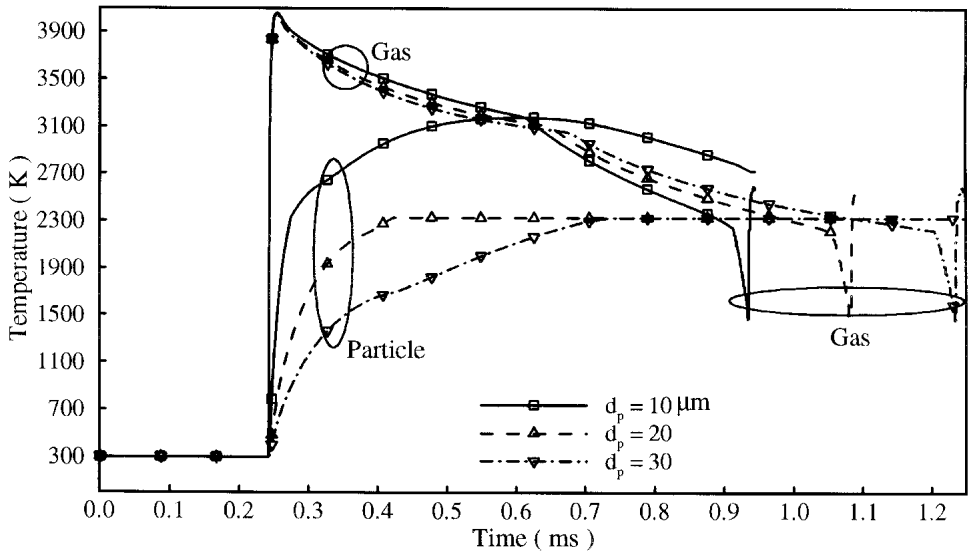

Fig. 9 Particle temperature versus time and gas temperature at the particle location for axial loading distances $x_i/L = 0.6$ and radial loading distance $y_i/r = 0.05$ ($L = 1.0$ m, SOD = 1d)

3. Numerical Solution Method

A high-resolution shock capturing numerical method with a total variation diminishing (TVD) property is used to solve the gas phase governing equations, where the time splitting and flux vector splitting techniques are used in conjunction with a two-step Runge-Kutta TVD scheme due to Shu and Osher.[17] The non-homogeneous part of the gas phase governing equations as well as the particle equations are solved using the DIVPAG subroutine of the IMSL library.[18] Detonation is initiated by assuming that the ignition of the reactive mixture near the closed-end of the barrel raises the gas pressure and temperature and creates a discontinuity in the gas properties. The computations proceed from this initial state where the chemical reaction is activated and the initial discontinuity develops into a detonation front. Reflective boundary conditions are used at solid boundaries while transmissive boundary conditions are used at the open boundaries of the computational domain. The computational domain is extended in both axial and radial directions to include the flow regions outside the barrel and beyond the target plate, where the open boundaries are placed far enough to ensure that the flow is not influenced by the transmissive boundary conditions. The complete details of the numerical scheme, the initial and boundary conditions and the extension of the computational domain are available elsewhere[6] and are thus not repeated here.

4. Results and Discussion

The gas phase evolution and transients in PDTS systems were analyzed in a companion article,[19] where it was shown

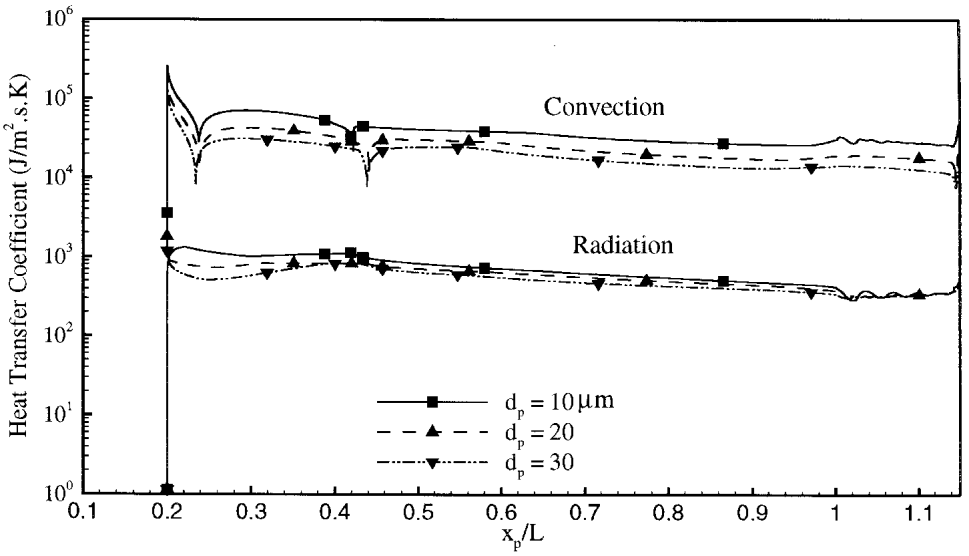

Fig. 10 Heat transfer coefficients versus particle axial location for particles of different sizes loaded at $x_i/L = 0.2$, $y_i/L = 0.05$ ($L = 1.0$ m, SOD = $6d$)

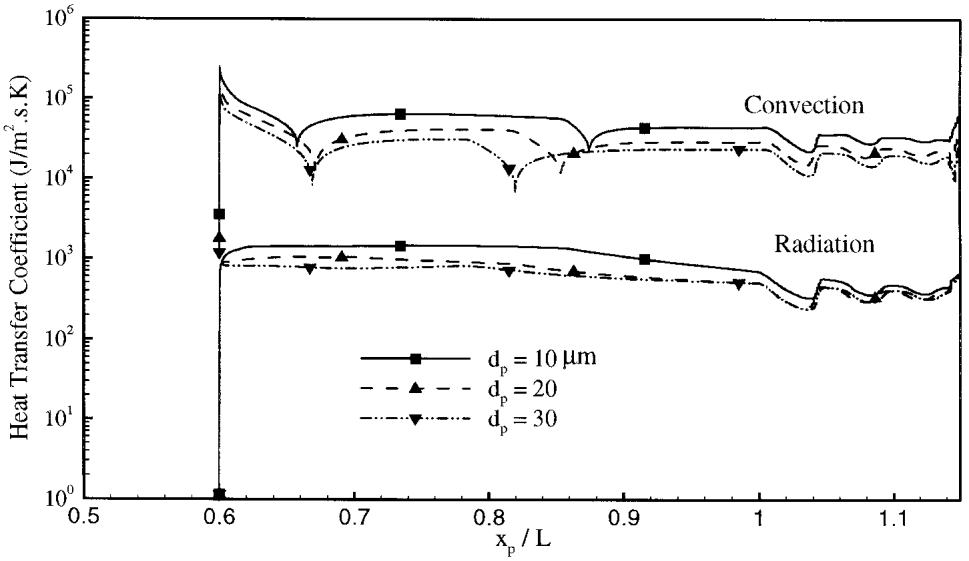

Fig. 11 Heat transfer coefficients versus particle axial location for particles of different sizes loaded at $x_i/L = 0.6$, $y_i/L = 0.05$ ($L = 1.0$ m, SOD = $6d$)

that the gas flow passes through many transient stages inside the barrel and after it exits to the surroundings. The focus of the analysis presented here is on the particulate phase dynamics and thermal analysis in PDTS systems. The reactive gas mixture used in this analysis is $C_2H_2/O_2/N_2$, with O/C = 1, $\%N_2 = 40$, and the resulting detonation wave speed for this mixture is 2464 m/s.[6] The detonation wave speed (D) is computed numerically at the Chapman-Jouguet (CJ) point at the Hugoniot of the reacted gas, $D = (u + a)_{CJ}$, u is the gas velocity, and a is the speed of sound.

The particle is assumed to melt over a range of temperatures about the particle melting point with $\Delta T_m = 1$ K. Several tube lengths are considered in this study while the tube diameter is taken as $d = 0.025$ m.

The most important parameters of interest as far as the particulate phase is concerned are the velocity and the percentage melt of the particle at the instant the particle reaches the target surface. The particle velocity at impact on the target surface should be high enough to achieve high hardness and low porosity coating layer. Also, the particle percentage melt is of primary importance since, if a particle reaches the target surface in its solid state it can bounce back, and if completely melted, it may splash. The particles should all have near-uniform velocity and percentage melt upon impact on the substrate to achieve a coating layer with uniform properties.

4.1 Internal and External Particle Dynamics

To see how a solid particle responds to gas flow in PDTS, the particle velocity and temperature are plotted against the particle

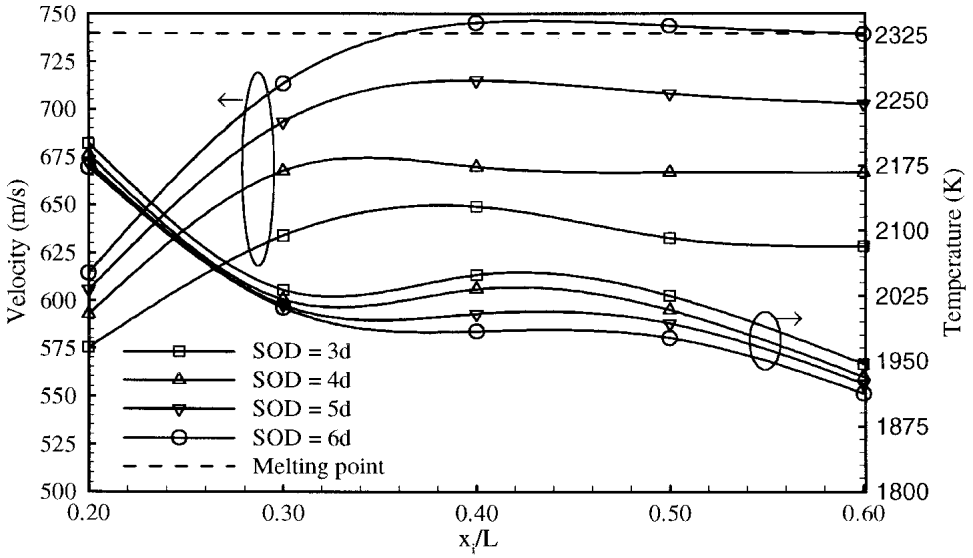

Fig. 12 Particle velocity and temperature at impact on the target plate versus axial loading location for $L = 0.5$ m ($d_p = 30$ μm, $y_i/r = 0.05$)

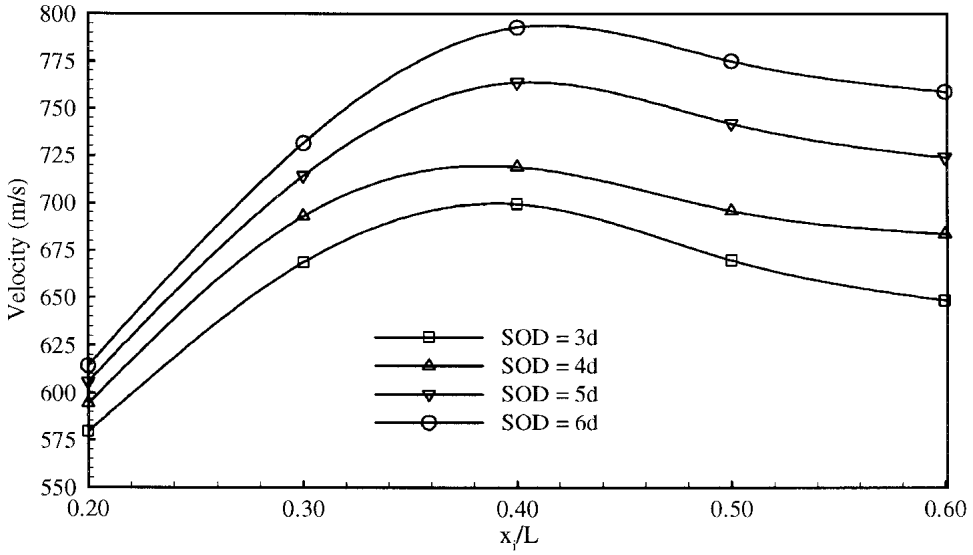

Fig. 13 Particle velocity at impact on the target plate versus axial loading location for $L = 0.75$ m ($d_p = 30$ μm, $y_i/r = 0.05$)

axial location (Fig. 2-5) in the gas stream from the initial loading position to the terminal location at the substrate for different particle sizes and initial loading locations. The gas velocity and temperature at the location of the particle is also shown on the same plots. The stand-off distance taken for this case is six tube diameters. The substrate in this case is far enough from the barrel exit plane so that the gas expands freely, where the exiting shock wave reaches the plate with a vanishing strength[6] leading to negligible shock reflection effects.

It may be noticed from these plots that for the particle sizes and the initial loading locations chosen, the solid particle experiences a typical behavior that may be described as follows. At the instant the detonation front passes by the particle, the particle is put in motion and is accelerated to a high velocity (Fig. 2 and 4). At the same time, the particle is suddenly heated up by the hot gases to a high temperature that, depending on the injection location, the particle temperature may reach the melting point (Fig. 3 and 5). After the passage of the detonation front, the particle falls in the expansion zone and continues to accelerate in that portion of this zone where the gas velocity is still higher than that of the particle. The particle then starts decelerating in the remaining portion of the expansion zone where the gas velocity becomes lower than that of the particle. Meanwhile the particle temperature continues to increase for most of the expansion zone width. The continuous increase in the particle temperature in this zone is due to the fact that the hot gases are still at a higher temperature than the particle and thus the particle temperature continues to increase attempting to equilibrate with the hot gases (Fig. 3 and 5). The velocity to which the particle decelerates in the expansion zone clearly depends on the particle size as well as

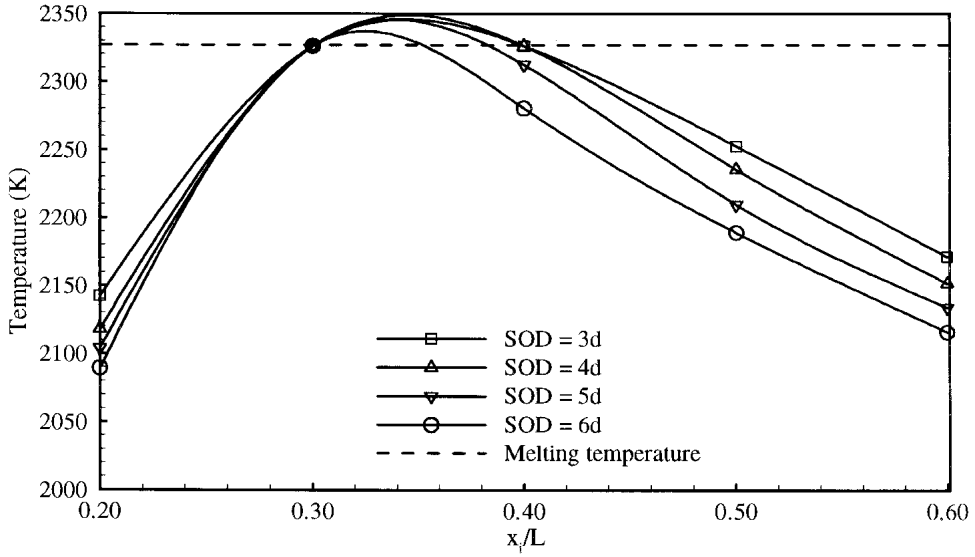

Fig. 14 Particle temperature at impact on the target plate versus axial loading location for L = 0.75 m (d_p = 30 μm, y_i/r = 0.05)

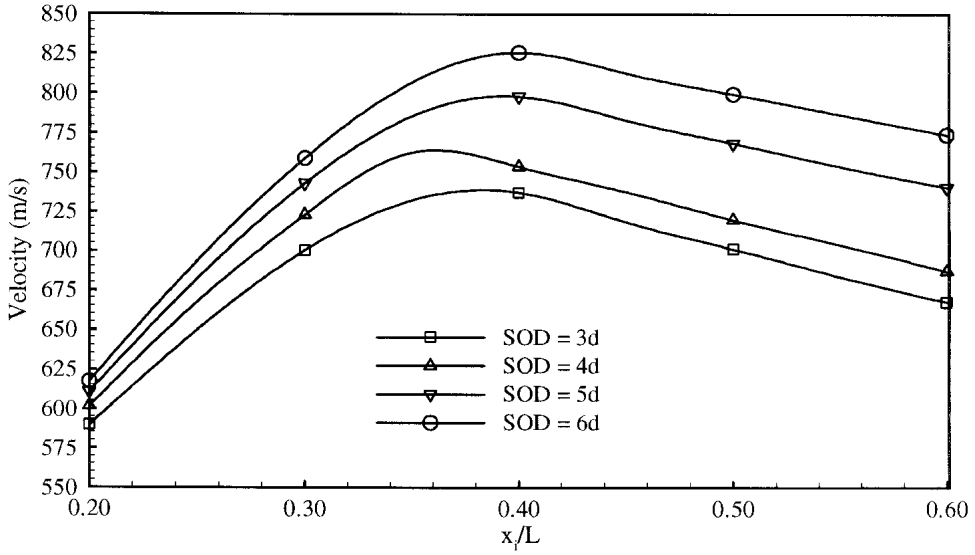

Fig. 15 Particle velocity at impact on the target plate versus axial loading location for L = 1.0 m (d_p = 30 μm, y_i/r = 0.05)

on its initial loading location. For example, the 10 μm particle with an initial loading location of $x_i/L = 0.2$ decelerates to almost a zero velocity. It may be noticed that after the passage of the detonation front, the 10 μm particle accelerates to about 880 m/s and then decelerates to almost zero velocity after the passage of the expansion zone, while the 20 μm particle (with the same loading location $x_i/L = 0.2$) accelerates to about 550 m/s then decelerates to about 100 m/s, and the 30 μm particle accelerates to 400 m/s and decelerates to about 150 m/s. This is in agreement with the fact that the smaller the size of the particle the easier to accelerate and to decelerate and vice versa, where the kinetic energy (for a spherical particle) is proportional to the third power of its diameter. It may also be noted that, for the same particle size, the maximum particle velocity attained after the passage of the detonation front is almost the same regardless of the initial loading location.

After the passage of the detonation front and the expansion zone where a particle reaches it minimum velocity inside the barrel, the particle starts to accelerate due to the start of the blow-down process during which the gas accelerates again. The gas temperature at the particle instantaneous location continues to decrease and, depending on whether the particle temperature has exceeded its melting temperature range, the particle temperature starts to decrease at the instant when the gas temperature becomes less than that of the particle.

As soon as the particle exits the barrel, it enters within the transient expansion-compression zone outside the tube. The gas exiting the tube experiences a series of successive interacting expansion and compression waves with considerable fluctuations in the gas velocity and temperature. The corresponding gas temperature in this region drops down below that at the barrel

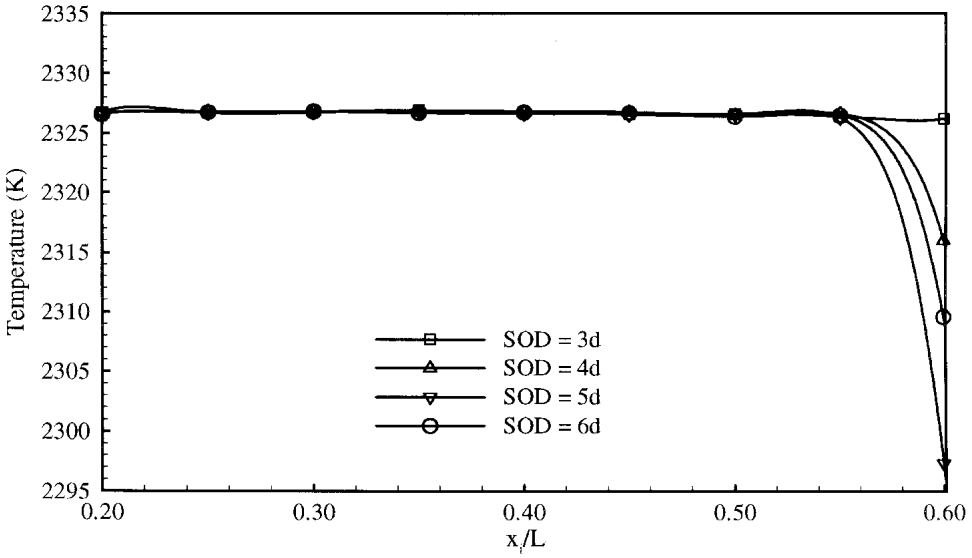

Fig. 16 Particle temperature at impact on the target plate versus axial loading location for $L = 1.0$ m ($d_p = 30$ μm, $y_i/r = 0.05$)

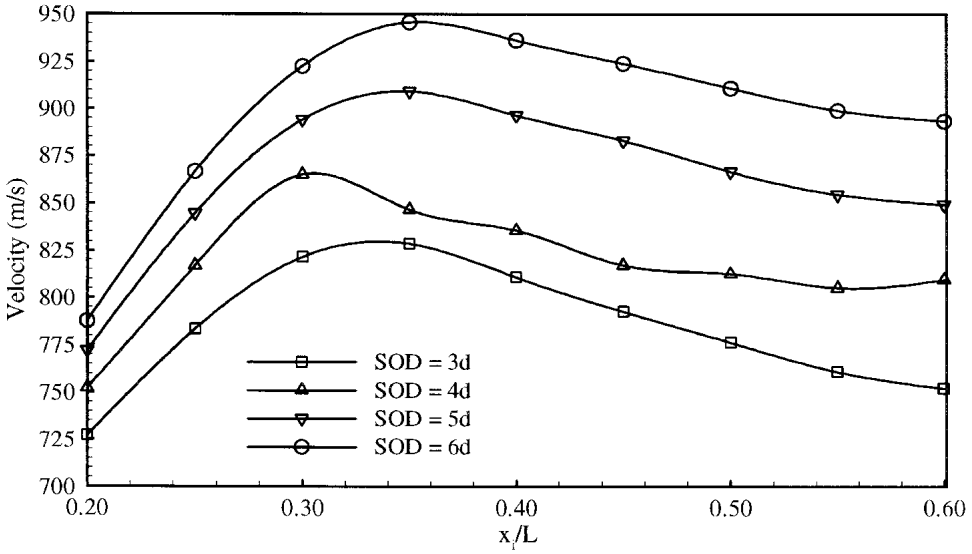

Fig. 17 Particle velocity at impact on the target plate versus axial loading location for $L = 0.75$ m ($d_p = 20$ μm, $y_i/r = 0.05$)

exit plane due to gas expansion and also fluctuates between minimum and maximum values. At this stage, the particle continues to accelerate more rapidly toward the target, while its temperature continues to decrease due to the decrease in the gas temperature upon expansion. It may be noticed that the smallest particle is influenced most by the gas velocity and temperature fluctuations in the expansion-compression zone, while bigger particles are barely affected. The particle velocity continues to increase within the distance between the barrel exit plane and the target surface except in the very vicinity close to the target surface at which the gas velocity sharply drops to zero and consequently the particle slightly decelerates. This is clearer for the 10 μm particle than the other bigger particles. In the limit of in an infinitely small particle size, the particle continuously takes almost the same velocity as that of the gas surrounding it and consequently reaches the target surface at a vanishing velocity. It is clear from Figs. 3 and 5, that it is also possible that the particle can undesirably exceed its melting point by a large amount causing the particle to probably evaporate or at least enhance the particle oxidation by the surrounding oxygen, resulting in contaminated particles at impact on the target surface. On the other hand, for particles loaded at the same location, the larger particle always reaches the target plate at a lower velocity than smaller ones. Also, larger particles are more difficult to heat, and it is possible that such particles can reach the plate with temperatures lower than their melting points. All of these conditions result in poor thermal spraying, where the properties of the coating layer (i.e, hardness, bond strength, adhesion, porosity content, etc.) are dependent on the velocity and temperature at which particles reach the target surface. Thus, depending on the reactive mixture

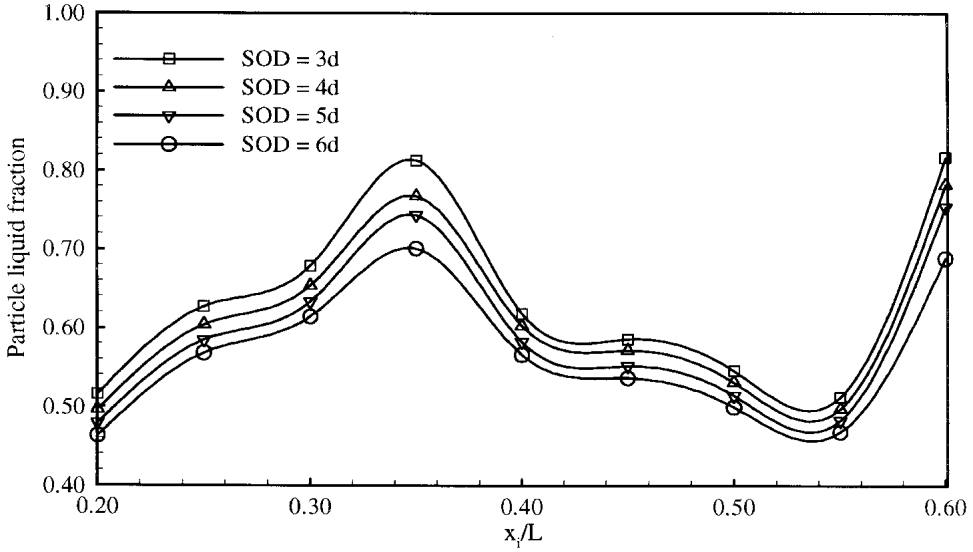

Fig. 18 Particle liquid fraction at impact on the target plate versus axial loading location for $L = 0.75$ m ($d_p = 20$ μm, $y_i/r = 0.05$)

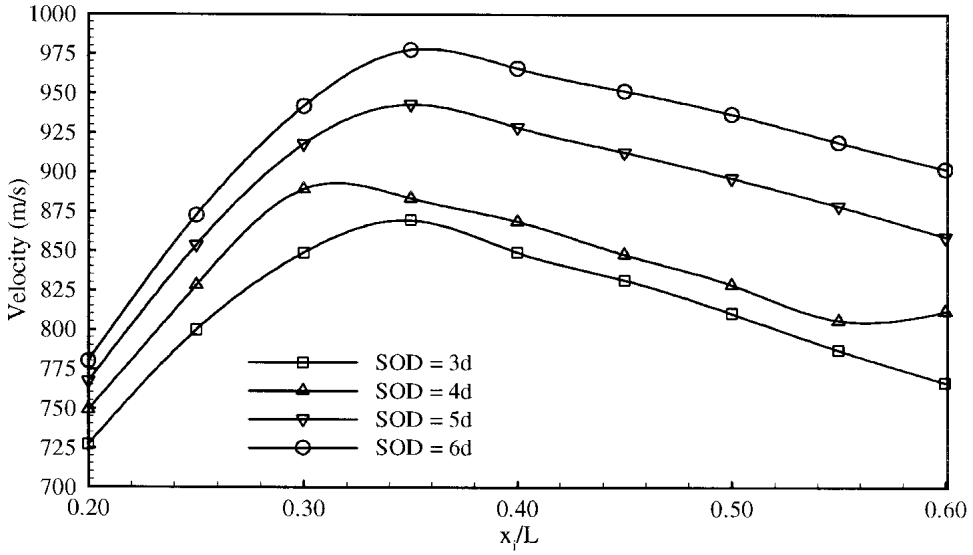

Fig. 19 Particle velocity at impact on the target plate versus axial loading location for $L = 1.00$ m ($d_p = 20$ μm, $y_i/r = 0.05$)

used, the PDTSA geometry and the solid particle properties as well as its loading position, there must be lower and upper limits on the particle size that may be used for efficient coating.

The other extreme case with regard to the stand-off distance is taken as one tube diameter in front of the barrel exit plane. As can be noticed from Fig. 6-9, the gas and particle profiles inside the barrel are qualitatively the same as in the case of SOD = 6*d* shown in Fig. 2-5, but the external field is much different. A stand-off distance of one tube diameter seems to be too small for the gas to expand freely outside the barrel. The gas expands at exit, and its velocity peaks in the vicinity of the exit plane, but it must drop to zero within 1*d* distance from the exit plane. Thus, there is not enough space for the expansion-compression series of waves to form and develop. This forms spiky velocity and temperature profiles between the barrel exit plane and the plate that looks like a standing shock wave and persists for a long time before it starts to diminish. The solid particle responds to this abrupt change in gas velocity, where it slightly accelerates then decelerates before it reaches the target (Fig. 6 and 8) while there is no noticeable variation in its temperature.

It can be deduced from Fig. 2-9 that the particle size, its initial loading and the stand-off distance are three important factors that affect the final state of the particle at impact on the target plate. Increasing the stand-off distance increases the external acceleration of the particle that adds up to that already gained internally, but at the same time decreases the particle temperature, where it is possible that a molten particle may freeze before reaching the target surface.

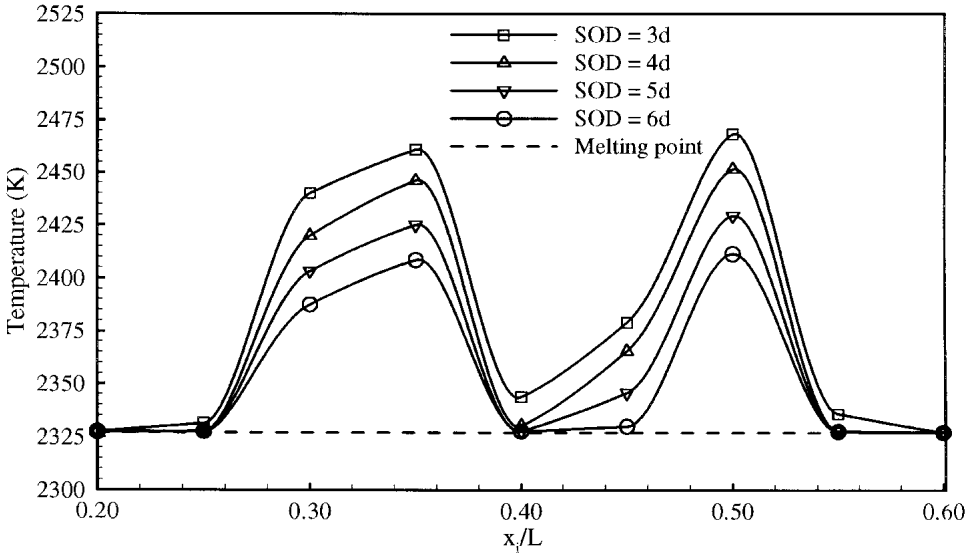

Fig. 20 Particle temperature at impact on the target plate versus axial loading distance for L = 1.00 m (d_p = 20 μm, y_i/r = 0.05)

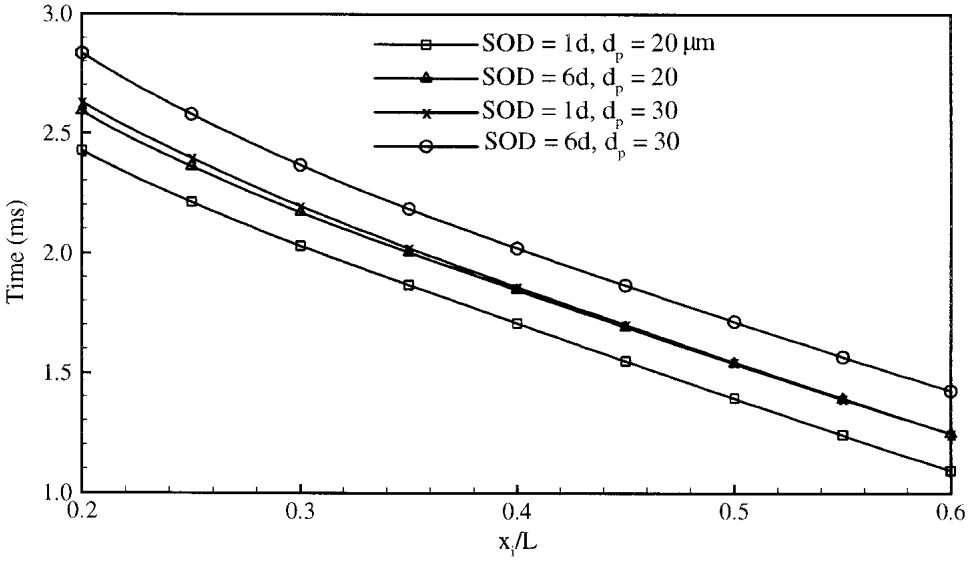

Fig. 21 Time required for particle to reach the target plate versus axial loading location for different particle sizes (L = 1.0 m, y_i/r = 0.05)

4.2 Convective and Radiative Heat Transfer

To see the relative effects of both convective and radiative heat transfer modes, the convective and radiative heat transfer coefficients are plotted against the particle location for the whole of the particle path (Fig. 10 and 11). The convective and radiative heat transfer coefficients are given by

$$h_{conv} = \frac{k}{d_p}(2 + 0.6Re_p^{1/2}Pr^{1/3}),\ h_{rad} = \varepsilon_p\sigma^*(T + T_p)(T^2 + T_p^2)$$

As can be seen from these plots, convection dominates over radiation heat transfer along the whole path of the particle. The convection heat transfer is about twenty to thirty times higher than radiation, except at the points where the particle-slip velocity (i.e., $|\vec{V} - \vec{V}_p|$) is minimum, where the Reynolds number drops drastically and so does the convective heat transfer coefficient.

4.3 Axial Loading Location and Stand-Off Distance Effects

Calculations were performed to analyze the effects of the stand-off distance on the particulate phase at impact on the target surface, and are presented in Fig. 12-20. Since this factor is interrelated with other important factors, such as the loading location, the barrel length and the particle size, all of these factors appear together in these plots. The tube length, the particle diameter, and the radial loading location are fixed as shown in these plots while the stand-off distance and the loading locations are varied. It is first noticed that for a barrel length $L = 0.5$ m, and particle diameter $d_p = 30$ μm (Fig. 12), the particle reaches the

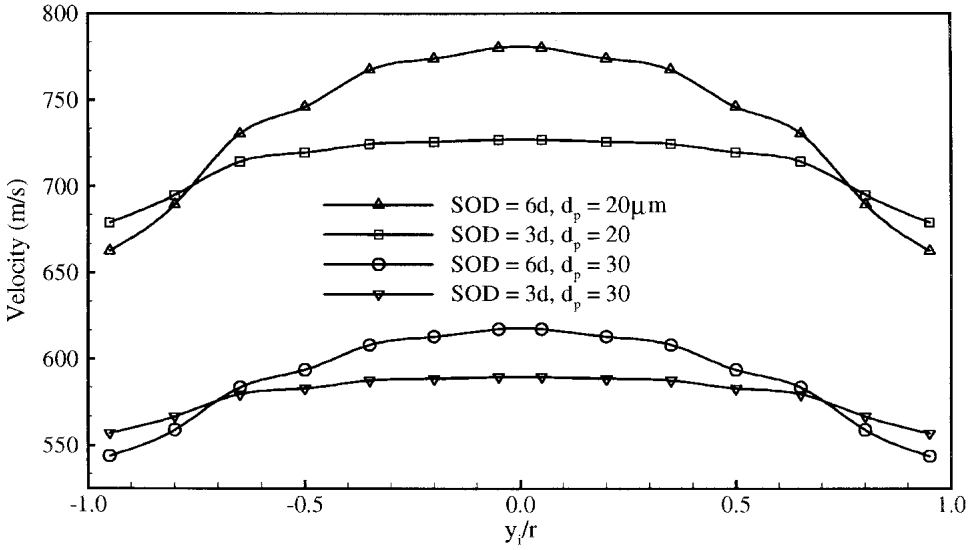

Fig. 22 Particle velocity at impact on the target plate versus its radial loading location for $L = 1.0$ m, $x_i/L = 0.2$

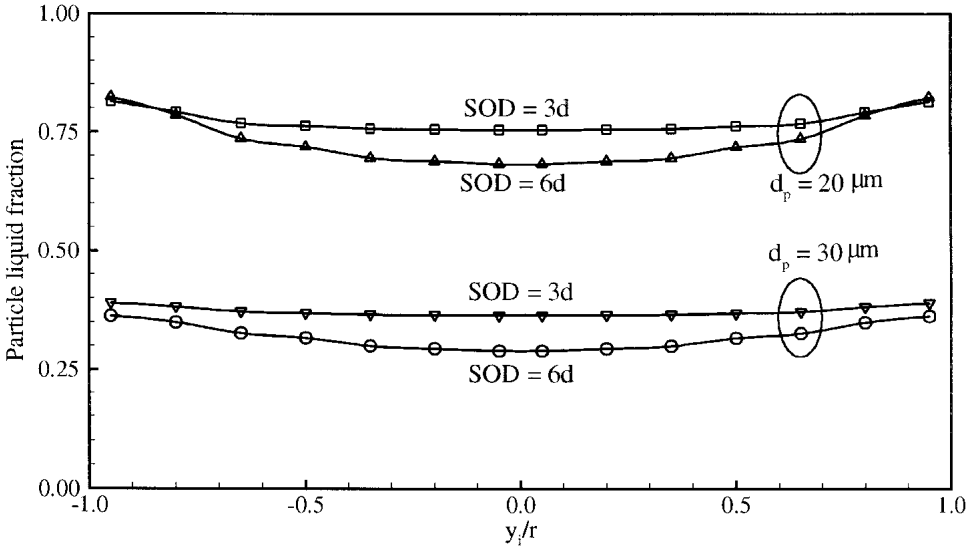

Fig. 23 Particle liquid fraction at impact on the target plate versus its radial loading location for $L = 1.0$ m, $x_i/L = 0.2$

target with a temperature less than its melting point, and consequently with a zero liquid fraction. This means that the solid particle is not given enough path in this case to reach the melting range.

The same calculations are repeated but for a barrel length $L = 0.75$ m (Fig. 13 and 14) as well as for $L = 1.0$ m (Fig. 15 and 16). The particle has reached the melting point only for some range of the loading distance for $L = 0.75$ m, and for almost the whole range with $L = 1.0$ m. The particle terminal velocity increases with increasing the stand-off distance, where increasing this distance increases the particle acceleration externally that adds up to the particle acceleration already gained inside the barrel. However, the maximum terminal particle velocity for a given stand-off distance is dependent on the axial loading location.

Calculations were also performed for a particle diameter d_p = 20 μm with tube lengths of 0.75 and 1.0 m. These are shown in Fig. 17-20. The same trend in the particle terminal velocity as for the case with $d_p = 30$ μm is noticed. The particle terminal temperature and liquid fraction are, however, different. For a tube length $L = 0.75$ m, the 20 μm particle reaches the melting point and there is a wide variation of the particle liquid fraction with the axial loading location, while for $L = 1.0$ m, the particle is exposed to excessive heating and its terminal temperature exceeds the melting point for most of the range of the axial loading locations shown and with strong dependence on the axial loading location.

Figure 21 shows the time required for the particle to reach the substrate for particle sizes 20–30 μm, and for a loading distance range of 0.2–0.6. The 30 μm particle loaded at $x_i/L = 0.3$ takes about 2.8 ms to reach the target surface. If each of the other stages in a PDTS applicator cycle takes about the same time,

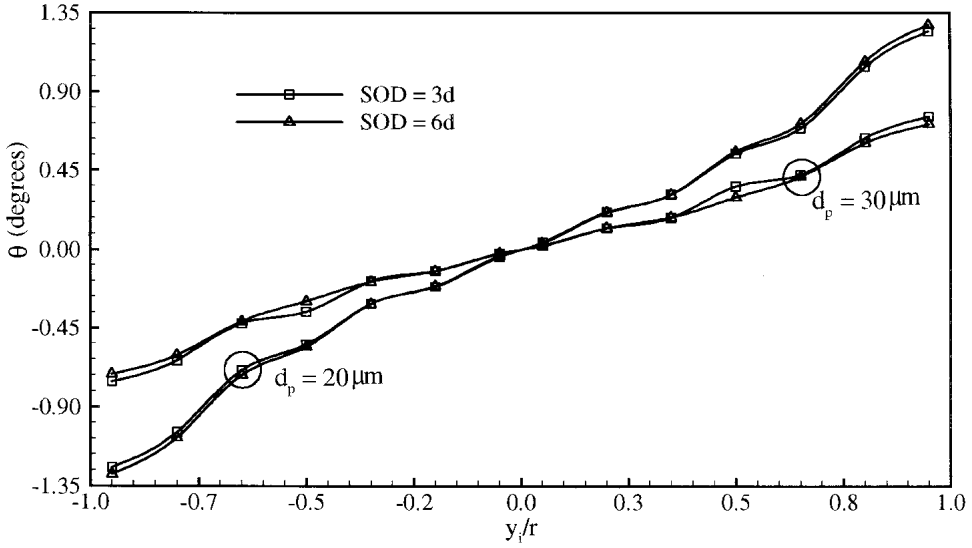

Fig. 24 Particle angle of incidence at impact on the target plate versus its radial loading location for $L = 1.0$ m, $x_i/L = 0.2$

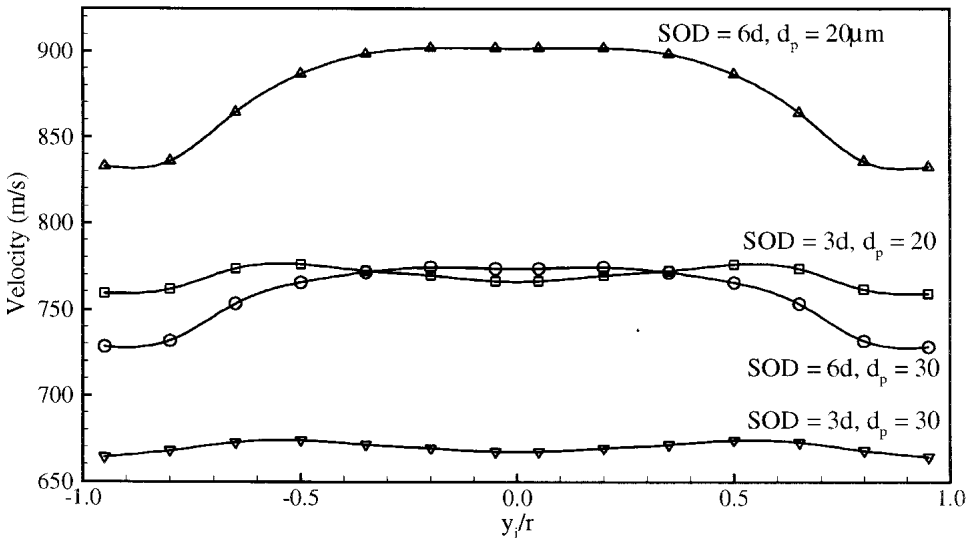

Fig. 25 Particle velocity at impact on the target plate versus its radial loading location for $L = 1.0$ m, $x_i/L = 0.6$

then a simple calculation shows that the firing frequency of a PDTS applicator can theoretically reach more than 100 cycles/s.

4.4 Radial Loading Location Effects

Particles loaded at different radial locations reach the target surface at different locations and with different conditions, and to achieve a coating layer with uniform final properties, particles deposited on the surface should reach the surface on all locations with minimum variations in their velocities and temperatures. Also important is the angle of incidence at which the particle reaches the target surface. The angle of incidence (θ) here is defined as the angle the particle velocity vector makes with the positive x axis (i.e., $\theta = \tan^{-1}[v_p/u_p]$). Particles reaching the target surface with higher angles of incidence have more tendencies to slip over the surface, and not to adhere to the surface properly. Several computations are performed to investigate the effect of the radial loading location on the uniformity of the particle terminal properties (velocity, liquid fraction and angle of incidence), and the results are shown in Fig. 22-27 for different parameters as shown in these plots. It is clear from these plots that decreasing the stand-off distance produces more uniform terminal particle velocities and liquid fractions, with negligible effect on the particle angle of incidence. Also particles with smaller diameters, result in less uniform terminal particle properties. For the axial loading locations chosen in Fig. 22-27 (i.e., $x_i/L = 0.2$ to 0.6), all the radial loading locations give near-uniform velocities and temperatures at impact on the target surface.

5. Conclusions

A numerical study of the particulate phase dynamics and thermal analysis in one cycle of pulsed detonation thermal spraying is presented using a two-component, compressible, re-

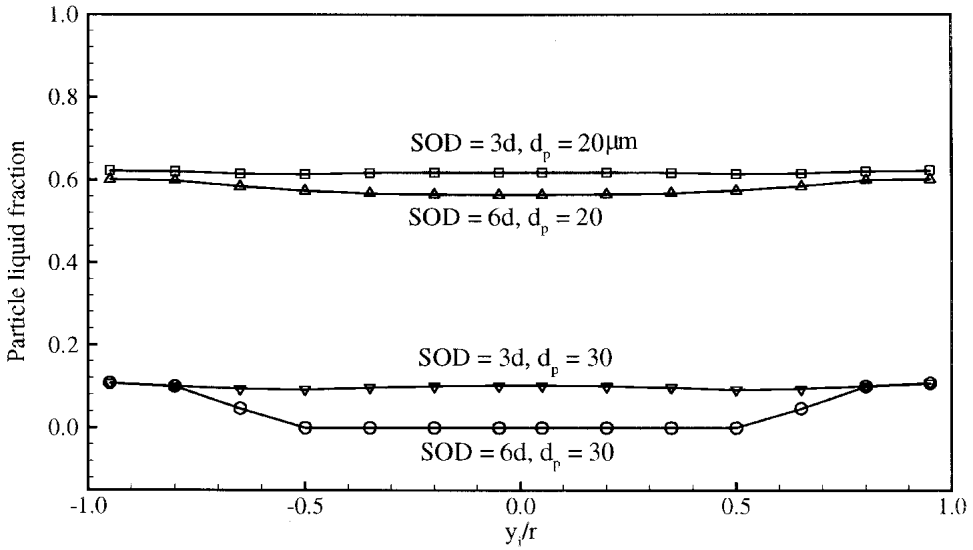

Fig. 26 Particle liquid fraction at impact on the target plate versus its radial loading location for $L = 1.0$ m, $x_i/L = 0.6$

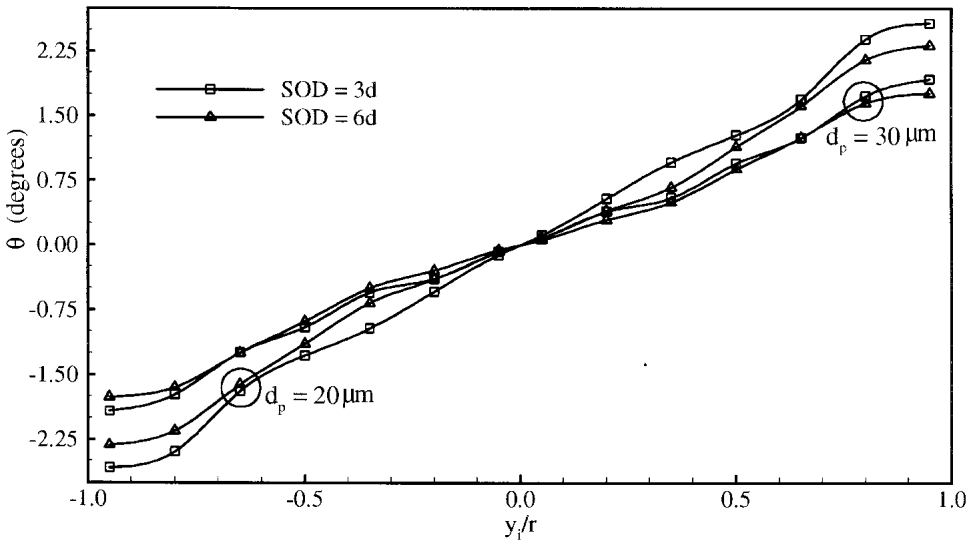

Fig. 27 Particle angle of incidence at impact on the target plate versus its radial loading location for $L = 1.0$ m, $x_i/L = 0.6$

active, two-dimensional, axisymmetric flow model, with a one-way coupling between the gas and the particulate phase. Due to the extreme transient effects in gaseous detonation spraying, the particle characteristics are very dependent on its instantaneous location in the gas stream. The analysis presented here shows that the geometrical configuration of the PDTS applicator, the particle size, and the loading locations are important parameters in determining the properties of the end product of a PDTS process.

In general, increasing the stand-off distance results in an increase in velocity and a decrease in temperature of the particle at impact on the target surface. Increasing the stand-off distance also results in less uniform properties of the coating layer where the properties of the coating layer are dependent on the particle characteristics upon impact on the target surface. The particle terminal velocity and temperature are strongly dependent on the particle axial loading location with a weak dependence on its radial loading location. To achieve a coating layer with uniform properties the powder material should be loaded over a narrow range of axial locations.

Since the gas flow in a PDTS process is extremely transient and passes through many stages during one cycle, the particle terminal properties are very much dependent on the instantaneous location of the particle in the gas flow field. This dictates that precise control needs to be exercised on the PDTS process variables for an efficient and optimized operation.

References

1. E. Kadyrov and V. Kadyrov: "Gas Dynamical Parameters of Detonation Powder Spraying," *J. Therm. Spray Technol.*, 1995, *4*(3), pp. 280-86.
2. E. Kadyrov and V. Kadyrov: "Gas Detonation Gun for Thermal Spraying," *Adv. Mater. Process.* 1995, *8,* pp. 21-24.
3. R.C. Tucker: "Detonation Gun Coatings," *J. Metals*, 1986, *38*(2), pp. 66-67.
4. M.K. Alkam and B. Butler: "Analysis of a Pulsed Detonation Thermal Spray Applicator," *Combust. Sci. Technol.* 2000, *159,* pp. 17-37.
5. P. Fauchais, A. Vardelle, and B. Dussoubs: "Quo Vadis Thermal Spraying?" *J. Therm. Spray Technol.*, 2001, *10*(1), pp. 44-66.
6. K. Ramadan: "A Computational Study of Pulsed Detonation Thermal Spraying," Ph.D. Thesis, The University of Iowa, Iowa City, IA, 2002.
7. M. Olim, O. Mond, M. Mond, and G. Ben-Dor: "A General Attenuation Law of Planar Shock waves Propagating into Dusty Gases" in *Proceedings of the 16th international Symposium on Shock Tubes and Waves*, H. Gronig, ed., Aachen, Germany, 1988, pp. 217-225.
8. G. Rudinger, *Fundamentals of Gas-Particle Flow,* Elsevier, NY, 1980.
9. S. Sivier, E. Loth, J. Baum and R. Löhner: "Unstructured Adaptive Remeshing Finite Element Method for Dusty Shock Flow," *Shock Waves*, 1994, *4,* pp. 15-23.
10. R.J. Gross, M.R. Baer, and M.L. Hobbs: "XCHEM-1D: A Heat Transfer/Chemical Kinetics Computer Program for Multilayered Reactive Materials," SANDIA Report SAN93-1603, Sandia National Laboratories, Albuquerque, NM, 1993.
11. E. Chang and K. Kailasanath: "Shock Wave Interactions With Particles and Fuel Droplet" in *38th Aerospace Sciences Meeting & Exhibit*, Reno, NV, 2000, AIAA-2000-0319.
12. E. Loth, S. Sivier, and J. Baum: "Dusty Detonation Simulations With Adaptive Unstructured Finite Elements," *AIAA J.*, 1997, *35*(6), pp. 1018-24.
13. R.G. Schmitt, P.B. Butler, and N. French: "Chemkin Real Gas: A Fortran Package for the Analysis of Thermodynamics and Chemical Kinetics in High Pressure Systems," UIME-PBB 93-006, University of Iowa, Iowa City, IA, December, 1993.
14. M.W. Chase, *NIST-JANAF Thermochemical Tables,* 4th ed., Parts 1 & 2, National Institute of Standards and Technology, Gaithersburg, MD, 1998.
15. C.R. Robert, J.M. Prausnitz, and B.E. Poling, *The Properties of Gases and Liquids*, 4th ed., McGraw-Hill, New York, 1987.
16. J.D. Anderson, *Hypersonic and High Temperature Gas Dynamics*, McGrow-Hill, New York, 1989.
17. C. Shu and S. Osher: "Efficient Implementation of Essentially Non-oscillatory Shock-Capturing Schemes," *J. Comp. Phys.,* 1988, *77,* pp. 439-71.
18. Microsoft Corporation, Fortran PowerStation Reference, 1995.
19. K. Ramadan and P.B. Butler: "Analysis of the Gas Flow Evolution and Shock Wave Decay in Detonation Thermal Spraying Systems," 2004, *13*(2).